JOURNAL OF THERMOPHYSICS AND HEAT TRANSFER
Vol. 16, No. 1, January–March 2002

Thermal Response and Inequivalence of Pulsed Ultraviolet-Laser Calorimeters

D. H. Chen*
University of Florida, Gainesville, Florida 32611
M. L. Dowell† and C. L. Cromer†
National Institute of Standards and Technology, Boulder, Colorado 80303
and
Z. M. Zhang‡
University of Florida, Gainesville, Florida 32611

This work investigates the thermal response of calorimeters that are used for measuring pulsed-laser energies at a wavelength of 193 nm, based on finite element models, and evaluates the inequivalence between laser heating and electrical heating. An axisymmetric model is built to study the thermal response of the cavity under both pulsed-laser heating and average-power (laser) heating. The small relative differences between pulsed-laser heating and average-power heating establish the feasibility of predicting calorimeter's thermal behavior for pulsed-laser heating by using the corresponding average-power heating. A three-dimensional finite element model of the entire cavity is developed and then used to predict the thermal response for average-power laser heating and electrical heating. The calibration factors (i.e., sensitivity factors) are obtained, and the inequivalence of the 193-nm laser calorimeter is calculated to be approximately 0.4%. The theoretical prediction provides a good reference for experimentally evaluating the inequivalence of the 193-nm pulsed-excimer-laser calorimeters.

Nomenclature

a	=	absorption coefficient, m^{-1}
b	=	$D/2\sqrt{(\ell n 2)}$, m
C_1	=	constant defined in Eq. (2)
C_2	=	constant defined in Eq. (7)
c_p	=	specific heat, J/kg K
D	=	full width at half-maximum (FWHM) beam diameter, m
D_1	=	diameter of laser beam, m
E	=	total deposited energy, J
f	=	pulse repetition rate, Hz
h	=	heat transfer coefficient, W/m^2 K
K	=	calibration factor, J/K
k	=	thermal conductivity, W/m K
m	=	mass, kg
N	=	inequivalence, Eq. (9)
N_a	=	relative difference to average-power laser heating, Eq. (4)
N_e	=	relative difference to electrical heating, Eq. (8)
P	=	heating power, W
Q	=	energy per pulse, J
$\dot{q}$	=	heat-generation rate per unit volume, W/m^3
R_g	=	reflectance at the glass surface
r	=	distance to the center of the laser beam, m
T	=	temperature, K
T_0	=	ambient temperature, K
t	=	time, s
v_s	=	speed of sound, m/s
x, y, z	=	spatial coordinates, m
α	=	thermal diffusivity, m^2/s
δ	=	thermal diffusion length, m
ζ	=	temperature rise $T - T_0$, K
η	=	cooling constant, s^{-1}
θ_1	=	incidence angle, deg
θ_2	=	refraction angle, deg
ρ	=	density, kg/m^3
τ	=	phonon relaxation time, s
τ_p	=	FWHM pulse width, s

Subscripts

a	=	average-power laser heating
c	=	copper
e	=	electrical heating
g	=	glass
p	=	pulsed-laser heating
ss	=	steady state

Received 12 April 2001; presented as Paper 2001-2759 at the AIAA 35th Thermophysics Conference, Anaheim, CA, 11–14 June 2001; revision received 10 September 2001; accepted for publication 8 October 2001.

*Research Assistant; currently Guest Scientist, Optical Technology Division, National Institute of Standards and Technology, Gaithersburg, MD 20899. Member AIAA.

†Project Leader, Sources and Detectors Group of the Optoelectronics Division.

‡Associate Professor, Department of Mechanical Engineering. Senior Member AIAA.

Introduction

CALORIMETERS, known for long-term stability and high overall accuracy, have been widely used to measure laser energy and power since the early 1970s. An isoperibol laser calorimeter consists of an absorbing cavity surrounded by a constant-temperature heat sink.[1] Electromagnetic energy from a laser is converted into thermal energy (i.e., internal energy) in the absorbing cavity. The amount of laser-induced thermal energy is determined by integrating the temperature difference between the cavity and the ambient over a specific time interval. An electrical heater attached to the absorbing cavity provides a means to calibrate the response of the calorimeter in electrical units. This eliminates the requirement for precise measurements of a calorimeter's thermal properties and provides direct traceability of laser energy to electrical standards.[2] Calorimeters have been designed to operate at

specific wavelengths and power/energy levels by careful geometric design and selection of appropriate absorbing materials in the cavity.[3] Surface-absorbing materials, such as black paints, have been widely used in calorimeters for continuous-wave (cw) measurements at low power.[1] However, surface-absorbing materials are usually not appropriate for use with pulsed lasers because for high pulse energies the peak temperature rise could degrade or damage the materials. For this reason volume-absorbing materials, which distribute the absorbed energy over a larger volume, are used in calorimeters for pulsed-laser measurements.[4]

The advent of laser-based photolithographic tools have generated a need for the construction of calorimeters and associated calibration systems for measurements of pulsed-laser power and energy for KrF (248-nm) excimer lasers at the National Institute of Standards and Technology (NIST).[5,6] The benefits of laser-based lithographic tools for integrated chip manufacturing are twofold: both shorter optical wavelength and narrower spectral bandwidth lead to smaller feature sizes, whereas greater average optical power translates into higher wafer throughput. Such lithographic tools, which employ KrF (248-nm) and now ArF (193-nm) excimer lasers, have led to an increased demand for accurate laser measurements in the deep ultraviolet (DUV) wavelength regime. Researchers at NIST have recently developed calorimeters and a second calibration system for excimer laser measurements at 193 nm (Ref. 7). Excimer lasers have been commercially available since the early 1970s and are widely used in a number of other applications in addition to semiconductor manufacturing, such as micromachining, materials processing, and photorefractive keratectomy (a common vision-correction procedure).[8–10]

Long-term exposure to high peak powers, high pulse energies, and short pulse widths from excimer-laser radiation damages most conventional optical materials. Hence, the NIST DUV calorimeters utilize carefully selected ultraviolet-absorbing glasses as the volume-absorbing material. The operating principles behind these calorimeters are similar to those for other previously developed isoperibol calorimeters used for pulsed-laser measurements.[1,3]

Our present study focuses on the thermal behavior of the cavity in the 193-nm calorimeter, shown in Fig. 1. The cavity is made of thin copper plate approximately 145 μm thick. The cross-sectional dimensions of the cavity are 3.5 × 3.5 cm. The inner surfaces of the cavity are coated with black paint (with an approximate thickness of 25 μm) to absorb any laser energy that is not absorbed by the glasses. The outer surfaces are gold-plated to minimize loss by radiative heat transfer. The thickness of this plating is approximately 5 μm. There are two volume-absorbing glass plates inside the cavity: one is epoxied to the back wall and the other to a side wall. The dimensions of each glass plate are 3.2 × 3.7 cm, and the thickness is 0.05 cm. The absorption coefficient of the glass is approximately 100 cm^{-1} at the wavelength of 193 nm. An electrical heater is attached to the outside surface of the back wall. The heater ring is made of copper with an inner diameter of 1.1 cm, an outer diameter of 2.8 cm, and a thickness of 0.05 cm. The surface of the heater ring is also gold plated. The heater ring is soldered to the cavity from the inner circumference, with a 0.05-cm gap between the heater ring and the back wall of the cavity. The gap is filled with heater wires and thermally conducting epoxy.

The cavity is suspended inside the isothermal heat sink by four stainless-steel tubular supports, and the whole calorimeter is purged

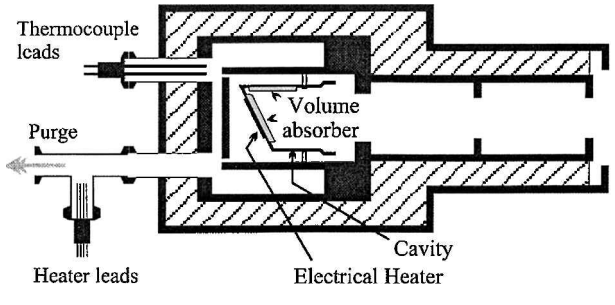

Fig. 1 193-nm laser calorimeter.

Table 1 Density, thermal conductivity, and specific heat of cavity components

Material	ρ, g/cm^3	k, W/cm K	c_p, J/g K
Glass	2.3	0.0073	0.7
Copper	8.933	4.01	0.385
Gold	19.3	3.17	0.129
Stainless steel	8.055	0.151	0.48
Ni-Cr alloy	8.6	0.19	0.43
Cu-Ni alloy	8.9	0.23	0.38

by nitrogen gas. Each support is 1.27 cm long and has an inner diameter of 0.16 cm and outer diameter of 0.21 cm. The relative temperature of the cavity is monitored by 20 type-E thermocouples whose junctions are epoxied to the outside surface of the cavity side walls and to the heat sink, which is held at a constant temperature of 303 K. The thermocouples are uniformly distributed on the outside surfaces of the side walls of the cavity and connected in series to improve the signal-to-noise ratio. Referring to Fig. 1, there are five thermocouples on each of the vertical plates, four thermocouples on the bottom plate, and six thermocouples on the top plate. Because of the different locations, lengths of the thermocouple wires vary slightly. The sensitivity of each thermocouple is 61.391 μV/K. The positive thermoelement is made of Ni-Cr alloy, and the negative thermoelement is made of Cu-Ni alloy.[11] The important thermophysical properties of the glass, copper, stainless steel, gold, Ni-Cr alloy, and Cu-Ni alloy are listed in Table 1 (Refs. 12–14). The emissivity of the glass is 0.8 (Ref. 15) and that of the black paint is 0.86 (Ref. 16). The emissivity of the gold coating is taken to be 0.01.

Chen and Zhang[17] developed several thermal models, including one-dimensional, axisymmetric, and three-dimensional models for studying thermal mechanisms of the volume-absorbing material used in the 193-nm laser calorimeter. Only the glass plate and an attached copper plate were considered, and electrical heating mechanisms were omitted. These models did not take into consideration the thermal behavior of the full cavity. Different heating methods (i.e., laser heating vs electrical heating) can potentially cause different thermal responses, yielding different calibration factors. If the calibration factor obtained from electrical heating is used to calculate the laser energy during pulsed-laser heating, an error might arise as a result of the difference in thermal response for the same amount of energy with different heating methods. The relative difference in the calibration factors between laser heating and electrical heating is defined as inequivalence of calorimeter. The inequivalence is very important for establishing the accuracy of pulsed-laser calorimeters. This work determines the feasibility of modeling the pulsed-laser heating with average-power heating and predicts the inequivalence for the 193-nm calorimeter through modeling of the entire cavity.

Axisymmetric Modeling

Numerical Model

An axisymmetric model and a three-dimensional model of the cavity have been developed using finite element software, ANSYS Version 5.6 (Ref. 18). Under the same element sizes and time steps the axisymmetric modeling is about 15 times faster than the three-dimensional modeling (to be discussed later). A simplified axisymmetric cavity model is employed to predict the thermal response for laser heating, as shown in Fig. 2. The square glass plate at the back of the cavity (the primary absorber) is modeled as a circular disk, and the other glass plate (the secondary absorber) is modeled as a ring, both with the same volume and thickness (0.05 cm). The heat capacity of the gold coating and black paint are added to that of the cavity. The effective thickness of the cavity is approximately 153 μm. Because of the equivalent volume and thickness, the inclined rectangular back plate is modeled as a circular axisymmetric disk, and the cavity is simplified to a cylindrical shell although the cross section in the real calorimeter is square. The electrical heater and heater ring with their original dimensions are attached to the back of the cavity. For simplification, the supports and thermocouples are neglected in the axisymmetric model. Hence, the total heat

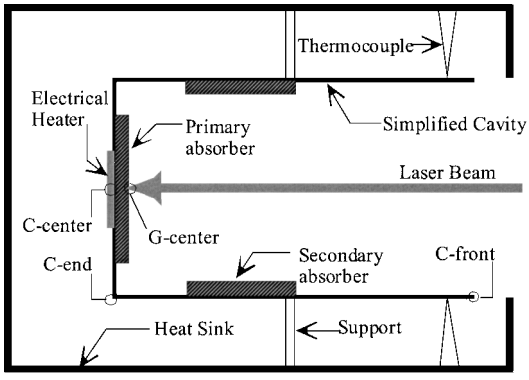

Fig. 2 Simplified axisymmetric cavity model. Ultraviolet-absorbing glasses were used as the primary and secondary absorbers. G-center: the center of the glass surface; C-center: the center of the cavity end; C-end: the edge of the cavity end; C-front: the front opening of the cavity.

capacity of the simplified axisymmetric cavity is the same as that of the sum of the actual cavity, two glass plates, and the electrical heater with ring. In Fig. 2, G-center refers to the center of the glass plate, C-center refers to the center of the outside surface of the back wall, C-end refers to the edge of the cavity end, and C-front refers to the front opening of the cavity.

For the pulsed-laser heating and average-power heating the heat-generation rate in the glass plate caused by the absorbed laser energy is approximated by a Gaussian distribution in the r direction and an exponential decay function in the z direction:

$$\dot{q}_1(r, z) = C_1 e^{-r^2/b^2} e^{-az} \tag{1}$$

where[19]

$$C_1 = \frac{a(1 - R_g)P}{\pi b^2} \tag{2}$$

To model pulsed-laser heating, the laser power is taken as a step function within τ_p (the FWHM pulse width) and $P = Q/\tau_p$. The actual pulse shape might be better approximated as Gaussian distribution in time; however, the step function results in almost the same temperature rise after the pulse because the thermal response within τ_p is essentially adiabatic.[17] To model average-power laser heating, the laser power is assumed to be continuous and $P = Qf$.

For short-pulse laser heating the validity of the Fourier heat-conduction equation should be examined. The Fourier equation is questionable when the phonon relaxation time τ is comparable to or greater than the pulse width (τ_p) (Ref. 20). From kinetic theory the relaxation time can be expressed as $\tau = 3\alpha/v_s^2$, where $\alpha = k/\rho c_p$ (Ref. 21). With $v_s = 5640$ m/s (Ref. 22) the phonon relaxation time in the glass determined by the preceding equation is on the order of 10 fs, that is, $\tau \ll \tau_p$. Hence, the Fourier heat-conduction equation is appropriate for studying the thermal response of the glass and copper components under excimer-laser heating.

The heat-conduction path and convection area in the axisymmetric model are approximately the same as those in the actual cavity. Heat is transferred from the cavity to the heat sink through convection and radiation only because conduction through the leads and supports are orders of magnitude smaller than convection. Here, the convection coefficient is estimated to be 8 W/m^{2}K, based on the correlation for natural convection with typical temperatures predicted under adiabatic conditions.[12] The view factor from the cylindrical surface to the cavity opening (i.e., the fraction of radiant energy leaving the side surface that arrives at the opening) is estimated to be 0.141 and that from the end surfaces to the opening is estimated to be 0.079 (Ref. 12). These view factors are used to calculate radiative heat loss from the inner walls, whereas the emissivity of the gold coating is used to calculate the radiative heat loss from the outer surfaces of the cavity. The radiative heat transfer between the interior surfaces does not contribute to the energy loss, and heat transfer between the cavity walls is dominated by conduction. Hence, the radiative heat exchange between inner surfaces is neglected. Equal temperatures and heat fluxes are used at the interface between the glass and copper (i.e., the boundary resistance is neglected). The initial temperatures of the glass and copper are set equal to the ambient temperature $T_0 = 300$ K. The generalized trapezoidal rule is employed for solving the equations, and the transient integration parameter is set to 1.0, at which the solution is unconditionally stable.

The element sizes and the time steps are carefully selected to achieve an acceptable accuracy within a reasonable computational time. The fine meshing is applied to the primary absorber in which the element sizes are from 0.025 to 0.09 cm in the r direction and from 0.001 to 0.005 cm in the z direction. Variable time steps are used for modeling heating and cooling processes. The relative error in the temperature predicted by modeling is about 5% compared with the theoretical calculation. For heat-generation rate with Gaussian distribution in space, the accuracy of the model is strongly dependent on the element sizes. However, the modeling result is very stable when the element sizes and the time steps are reduced by half, and an extremely high absolute accuracy is not necessary because the objective of using the axisymmetric modeling is to predict the relative difference between pulse heating and average-power heating.

The finite element model is further verified under adiabatic conditions, where the final temperature rise is the ratio of the deposited energy to the total heat capacity of the cavity. For the adiabatic boundary condition the steady-state temperature rise of the glass and copper disks can be easily calculated from the following equation:

$$[(mc_p)_g + (mc_p)_c]\zeta_{ss} = (1 - R_g)E \tag{3}$$

When R_g is set to zero and the total pulse energy E is equal to 12 J, the uniform temperature rise ζ_{ss} from Eq. (3) is 1.411 K. The predicted temperature rises after 200 s for the pulsed-laser heating and for the corresponding average-power heating are equal to the theoretical value. This indicates that the deposited energies in the models are correct.

Results of the Axisymmetric Modeling

For pulsed-laser heating with a pulse energy of 50 mJ, the maximum energy of 12 J limits the number of pulses to 240 pulses over an interval of 2.4 s at a repetition rate of 100 Hz. The heat source is turned off at 2.4 s, and the modeling extends to 200 s. In the following discussion the heating process refers to the first 2.4 s, and the cooling process refers to the time between 2.4 and 200 s.

The resulting temperature rises at different locations are shown in Fig. 3a. Figure 3b provides details of the initial temperature history at the center of the glass surface. Each pulse is modeled as a step function of heating source with 15-ns duration, and the temperature at G-center increases sharply during pulse heating and drops as a result of heat conduction until the next pulse. This explains the oscillatory feature observed in Fig. 3b. The temperature rise is the greatest at the center of the glass surface, where the heat-generation rate is the highest [see Eq. (1)]. The temperature of the center of the glass surface increases quickly at the beginning and slowly near the end of the heating process ($t = 2.4$ s), owing to the increasing heat losses by convection and radiation at the glass surface and heat conduction to other parts of the glass and copper. There is a large temperature difference between G-center and C-center because of the low thermal conductivity of glass. The heat conduction in copper is much larger than that from glass to copper. Therefore, the temperature at C-center drops almost at the same time as that of G-center. The temperatures at the edges continue to increase until they reach almost the same temperature as the centers.

In the average-power heating the heating process is modeled with a continuous (i.e., nonfluctuating) power source. The heat-generation rate is given in Eq. (1) during the heating process with $P = Qf$. For a laser pulse energy of 50 mJ and repetition rate of 100 Hz, the power for the corresponding average-power laser heating is 5 W, the heating time is 2.4 s, and the cooling process is calculated up to 200 s. As shown in Fig. 4, the maximum temperature rises at the centers of the glass and copper are 109.3 and 17.2 K,

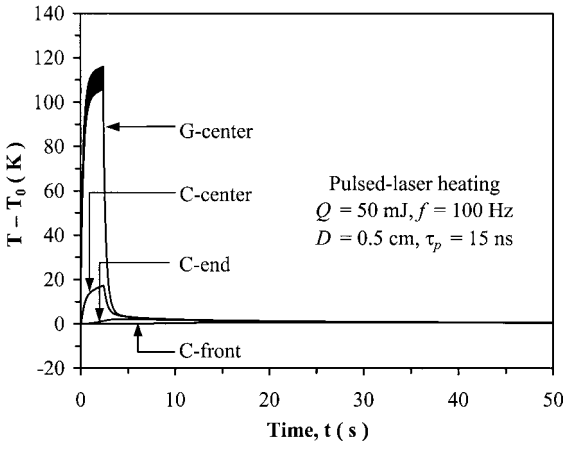

a) Heating and cooling process

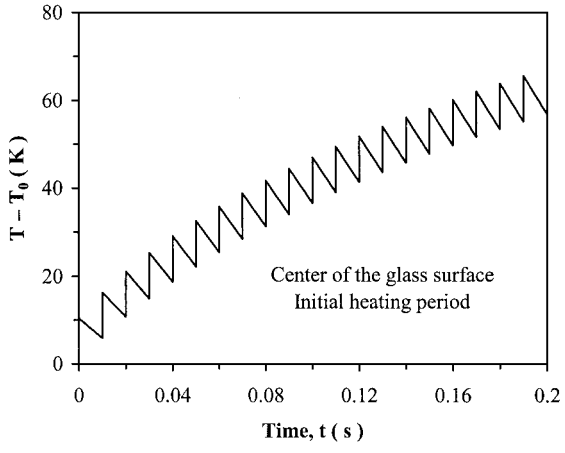

b) Initial heating period

Fig. 3 Temperature histories for pulsed-laser heating.

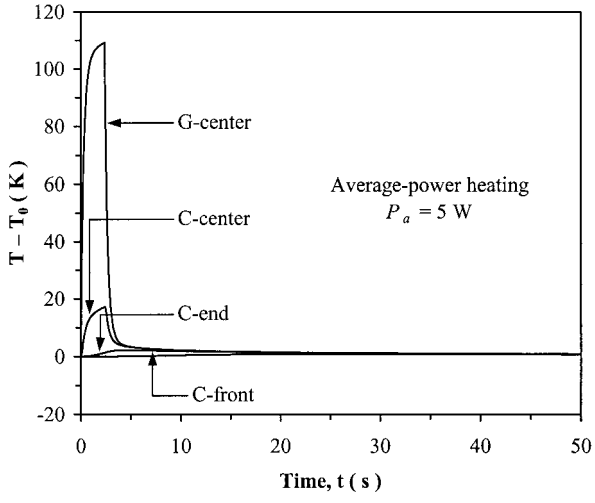

Fig. 4 Temperature histories for average-power heating.

respectively. Variations of the thermophysical properties of glass are neglected in the model. From 300 to 400 K, the thermal conductivity of glass increases by less than 5%, and the specific heat of glass increases by about 15% (Ref. 23). This suggests that the model can overpredict the peak temperature. The temperature trend in the cooling process is very similar to that of pulsed-laser heating. For example, the temperatures at G-center and C-center drop quickly at the same time. The temperature at C-front increases slowly until it is almost equal to those at the centers, and then the temperature of the whole cavity decreases slowly.

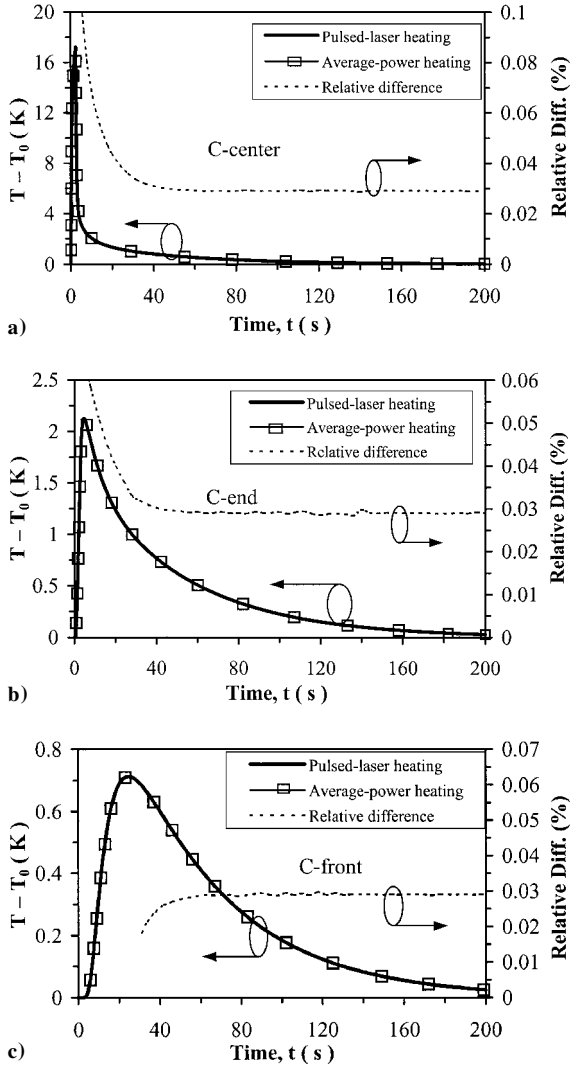

Fig. 5 Temperature history and relative difference at a) C-center, b) C-end, and c) C-front.

The relative difference N_a in the temperature rises ($\zeta = T - T_0$) for pulsed-laser heating, and average-power heating is defined as

$$N_a = \frac{|\zeta_p - \zeta_a|}{\zeta_a} 100\% \tag{4}$$

The temperature rises for pulsed-laser heating and average-power heating and their relative difference at C-center, C-end, and C-front are shown in Fig. 5.

At C-center N_a is large initially owing to the small temperature rise. The maximum temperature rises for pulsed-laser heating and average-power heating are 17.22 and 17.20 K, respectively, indicating N_a is 0.12%. As soon as the cooling process starts, the relative difference drops rapidly and remains constant (0.03%) after 40 s. The constant relative difference indicates the temperature decays exponentially after 40 s. A similar trend can be observed for C-end in Fig. 5b. At C-front N_a is initially small and increases to 0.03%, as shown in Fig. 5c.

Although the axisymmetric model is simple, it captures the most important characteristics of the cavity and provides the correct trends of the thermal response. This model, however, cannot predict the true temperature history and distribution because of the different geometric structures used. In general, the axisymmetric model overpredicts the relative difference as a result of the constant convection coefficient. Hence, the small relative difference demonstrates good equivalence between the cooling processes from the pulsed-laser heating and average-power heating for the equivalent deposited energy and heating time. To save computational time in the three-dimensional

modeling, the calibration factor of pulsed-laser heating can be obtained through modeling the corresponding average-power heating. The calibration factor is determined by the following equation[5,6]:

$$K = E \Big/ \left[(\zeta_2 - \zeta_1) + \eta \int_{t_1}^{t_2} \zeta(t)\, \mathrm{d}t \right] \tag{5}$$

where ζ_1 and ζ_2 are the average temperature rises of 20 thermocouples at times t_1 and t_2, respectively; t_1 and t_2 are times at which the output can be expressed as an exponential decay function. The equivalent cooling process indicates the same temperature difference from t_1 to t_2 and the same cooling constant. When times t_1 and t_2 are set to 0 and 200 s, the relative differences in the integration

$$\int_{t_1}^{t_2} \zeta(t)\, \mathrm{d}t$$

between pulsed-laser heating and average-power heating are 0.03% at C-end and 0.001% at C-front. Even when the time t_2 is reduced to 50 s, the relative difference in the integration remains 0.03%. Although the relative difference of the temperature rise during the heating process is larger than that during the cooling process, the integrated temperature rise from t_1 to t_2 is nearly the same. This is because the higher integrated temperature during the heating process causes a slightly larger energy loss, which results in a lower temperature in the cooling process.

Based on the analysis at C-end and C-front, a limit on the relative difference of the calibration factor between pulsed-laser heating and average-power heating can be set at 0.03% for a pulse energy of 50 mJ and a repetition rate of 100 Hz. The pulsed-laser heating with low repetition rate is closer to the corresponding average-power heating than that with high repetition rate, and hence, the inequivalence is smaller for lower repetition rates. In the next section the average-power laser heating is used in a three-dimensional model to predict the calibration factor corresponding to pulsed-laser heating.

Three-Dimensional Modeling

Three-Dimensional Model

A three-dimensional finite element method has been developed to predict the temperature histories at 20 thermocouple locations for calculating the calibration factors because the axisymmetric modeling cannot provide the true temperature history and distribution of the cavity. The finite element mesh is shown in Fig. 6. Although the copper and glass plates are very thin, three-dimensional solid elements are used instead of shell elements for the glass and copper in order to model the volumetric heat generation in the glass and electrical heater. The glass and copper plates are divided into several regular volumes for automatic meshing, and the adjacent volumes are connected through shared nodes on their interface. The circular electrical heater and heater ring are simplified to square rings with the same volumes as the actual rings. A conduction bar is used to model the heat conduction through the supports.

The laser beam is incident on the glass surface at the back of the cavity at an incidence angle of 30 deg. The diameter D_1 of the laser beam is 0.5 cm. In the model the laser intensity is approximated as uniform in space and with a square shape of the same cross-sectional area as the circular beam. The influence of the spatial distribution of the laser beam on the temperature history at the thermocouple locations is small. Of the incoming laser energy the primary absorber at the back of the cavity absorbs 96% and reflects 4% to the secondary absorber at the side wall, which absorbs 96% of the reflected radiation. The radiant energy leaving the secondary absorber is only 0.16% of the incoming laser energy and will essentially be absorbed by the black paint. In the model, however, all of the laser energy reflected by the primary absorber (4% of the incident energy) is treated as uniform heat generation inside the secondary absorber. Because the incident laser beam is not normal to the primary absorber, the transmitted laser beam is not perpendicular to the glass-copper interface. The heat generation rate $\dot{q}_2$ in the primary absorber is given as

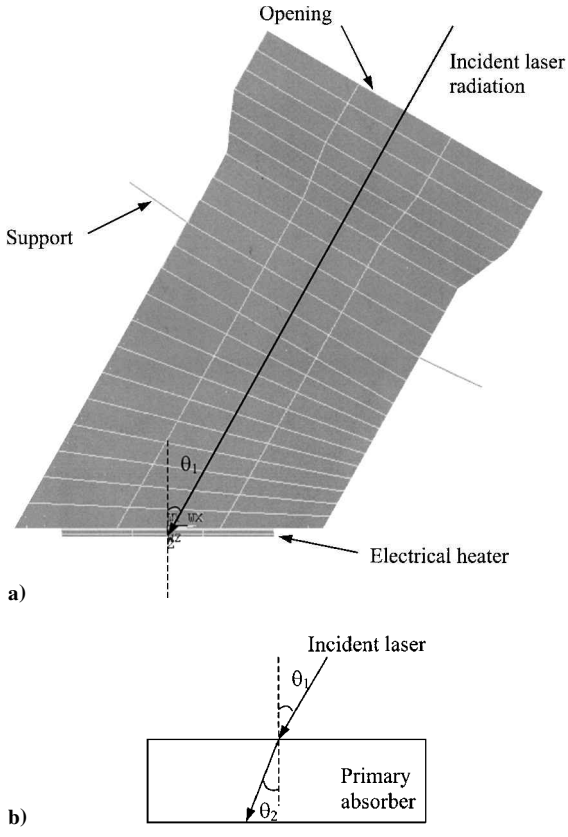

Fig. 6 Schematic of a) the cavity meshing and b) laser-absorber interaction. The orientation is different from Fig. 1.

$$\dot{q}_2(x, y, z) = C_2\, e^{-az/\cos\theta_2} \tag{6}$$

where[19]

$$C_2 = \frac{4a(1 - R_g) P \cos\theta_1}{\pi D_1^2 \cos\theta_2} \tag{7}$$

The refraction angle θ_2 is determined by Snell's law. Electrical energy is applied through heat generation within the heater volume, in which the uniform heat-generation rate is the electrical power divided by the heater volume.

Based on experimental data, the initial temperature is set to be the ambient temperature ($T_0 = 303$ K). In the theoretical model the temperature rise is relative to the ambient temperature of 303 K. The radiative heat transfer inside the cavity is modeled using a radiation matrix method. A space node representing the ambient is used to account for the radiative energy loss from the inner surface of the cavity. A convection boundary condition is applied to the inner and outer surfaces of the cavity, in which the convection coefficient is temperature dependent.

Available convection correlations fail to predict the convection coefficients in both the heating and cooling processes for the following reasons: 1) the cavity is enclosed by the heat sink with a small distance separating the two; 2) the geometry of the cavity is complicated with tilted, vertical, and horizontal plates; and 3) the temperature of the cavity is not uniform and changes with time, and the temperature rise is very small. At the beginning of the heating process, thermal diffusion in the nitrogen dominates the heat-transfer process. The thermal diffusion length δ can be calculated using $\delta = \sqrt{(\pi \alpha t)}$, and the heat-transfer coefficient h can be estimated as $h = k/\delta$. The heat-transfer coefficient can be very high initially but decreases as the thermal diffusion length increases. Natural convection starts to play a role when boundary layers are formed near the surfaces. Inside the cavity convection also carries heat from the inclined back

plate to the top plate. Near the end of the heating process, the nitrogen gas around the cavity has been warmed up. This results in a lower heat-transfer coefficient during the cooling process. In the computational modeling the convection coefficients are estimated from curve-fits to experimental measurements of electrical heating. Even though the temperature distribution and history for average-power laser heating are slightly different from those for the corresponding electrical heating, it is appropriate to use the convection coefficients obtained from electrical heating for the average-power heating because the model employs a linear interpolation. Because the temperature at the heating center is slightly higher for average-power heating than for electrical heating, the convection coefficients obtained from curve fitting are linearly extended and then used in the average-power laser heating.

The element size and time step have been tested and selected carefully. For the primary absorber the element size in the z direction is 0.001 cm for $0 \le z \le 0.01$ cm, 0.002 cm for $0.01 \le z \le 0.02$ cm, 0.005 cm for $0.02 \le z \le 0.04$ cm, and 0.01 cm for $0.04 \le z \le 0.05$ cm. Only one layer element is used for the secondary absorber. The element size in the x-y plane is 0.2 cm for the center volume with heat generation and 0.4 cm for the other domain. When the element size is reduced by 50%, the relative difference of the predicted temperature is about 0.8%. Different time steps are used in the heating and cooling process, and a very small time step (on the order of 10^{-12} s) is used at the beginning of the cooling process for numerical convergence. When every time step is reduced by half, the relative difference of the modeling result is less than 0.1%. Hence, the numerical solutions of the model with the current element sizes and time steps are stable. The adiabatic analysis also indicates that the deposited energies in the finite element model are correct for both average-power laser heating and electrical heating.

Results of the Three-Dimensional Model

In the experiments a 6-$\frac{1}{2}$ digit (22 bit) digital multimeter (DMM) of high accuracy measured the current through and voltage across the heater. A highly sensitive 7-$\frac{1}{2}$ digit DMM with a resolution of 0.1 nV measured the thermocouple output voltage. The energy injection time was 80 s, the settling time was 48 s, the final rating period was 120 s (The final rating period was used to fit the cooling constant using exponential decay function). And the sampling interval was 2 s. The integration period was from the initial time ($t_1 = 0$) to the beginning of the final rating period ($t_2 = 128$ s). The standard deviation of the calibration factor in the electrical heating experiments is less than 0.02% for injection energies of 5 J or greater.

Experimental data for electrical heating were compared with the simulated results to estimate the convection coefficients. The deposited energies were 9.022 and 5.008 J for different electrical power and the same heating time, respectively. The fitting process is converged when the relative difference in the cooling constants is less than 1%, and the relative difference in the calibration factors is less than 0.1%.

The fitted curve and experimental data with a deposited energy of 9.022 J are shown in Fig. 7a, in which $T - T_0$ is the temperature rise averaged over the 20 thermocouple locations. The fitted curve agrees very well with the experimental data. The relative difference of the cooling constant is 0.17%, and the relative difference of the calibration factor is 0.07%. The heat-transfer coefficient at the beginning of the heating process is on the order of 100 W/m^2 K owing to the small thermal diffusion length. With the development of boundary layers, the natural convection coefficient slowly approaches the theoretical prediction (2–3 W/m^2 K) at the end of the heating process. During the cooling process, the convection coefficient was about 1 W/m^2 K and changes slightly within 1%. This was caused mainly by heat diffusion from the outside surfaces of the cavity to the heat sink through the nitrogen gas. This can also be observed in the experimental data. The cooling constant was almost the same when the deposited energy was changed from 9 to 5 J. The convection coefficients obtained by fitting the experimental data were linearly extrapolated to model the corresponding average-power laser heating.

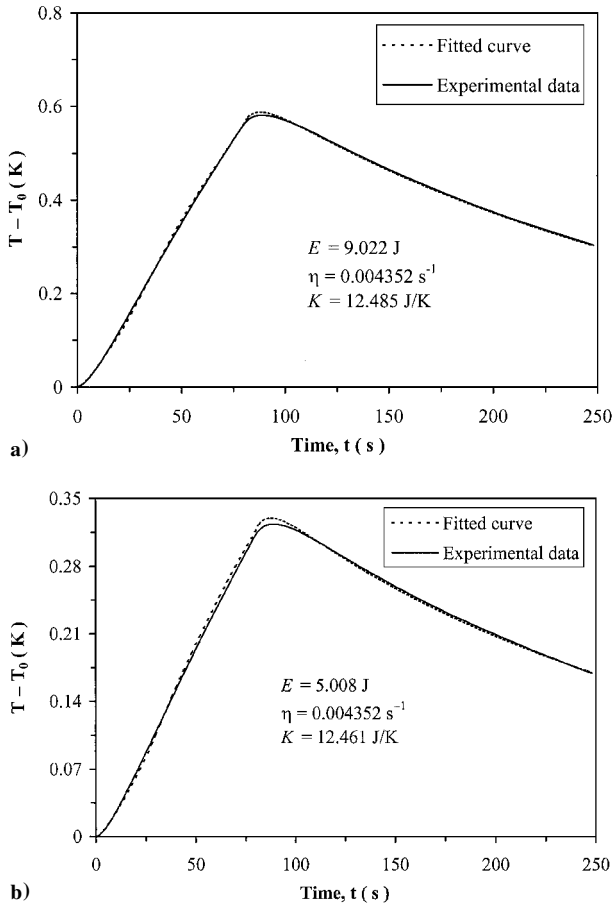

Fig. 7 Experimental data for electrical heating and fitted curve at deposited energy of a) 9 J and b) 5 J.

The fitted curve and experimental data at the deposited energy of 5.008 J are shown in Fig. 7b. The fitted curve follows the experimental data very well. The cooling constant was 0.004352 s^{-1}, which is 0.26% larger than the experimental value. The calibration factor predicted from the fitted curve was 12.461 J/K, which is 0.01% larger than the experimental result.

The convection coefficients obtained from fitting the experimental data of the electrical heating with the energies of 9.022 and 5.008 J were used to model the corresponding average-power laser heating. For average-power laser heating, the total deposited energy, the heating time, and the cooling time were the same as those for the corresponding electrical heating. The relative difference N_e in the temperature rise between average-power heating and electrical heating is defined as the following:

$$N_e = \frac{|\zeta_a - \zeta_e|}{\zeta_e} 100\% \tag{8}$$

The temperature histories and relative differences predicted by the three-dimensional model for average-power heating with energies of 9 and 5 J are shown in Fig. 8. At the beginning of the cooling process, the relative difference dropped quickly and then remained nearly constant during the cooling process. The cooling constant was the same as the corresponding electrical heating. The calibration factors were 12.537 and 12.511 J/K for average-power heating with energies of 9.022 and 5.008 J, respectively.

The inequivalence is the relative difference between the calibration factors for laser heating and electrical heating of the calorimeter. Hence, the inequivalence N can be calculated using the following:

$$N = \frac{|K_a - K_e|}{K_e} 100\% \tag{9}$$

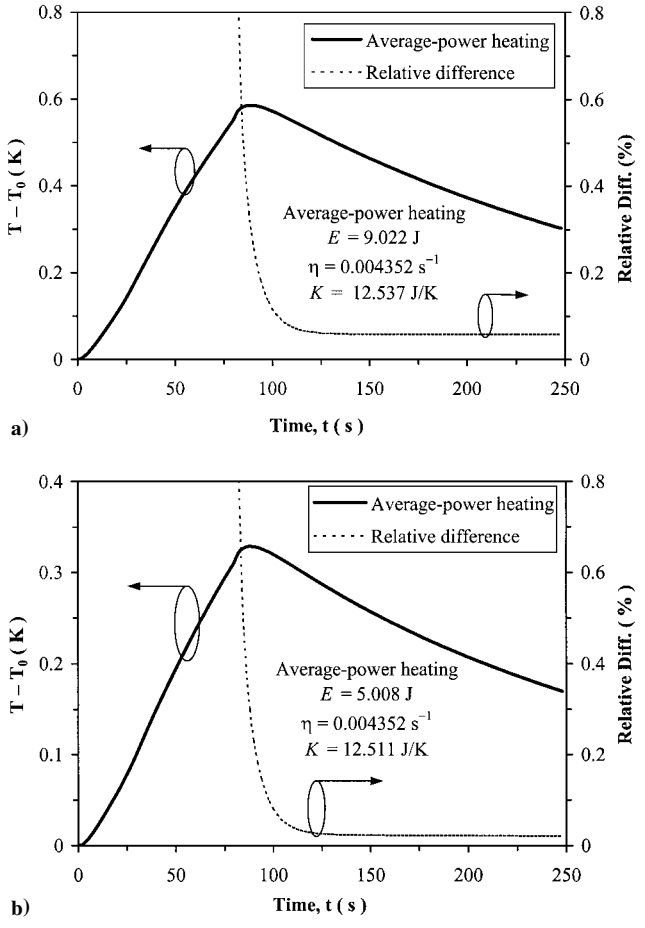

Fig. 8 Temperature rise for average-power heating at deposited energy of a) 9 J and b) 5 J.

where K_a and K_e are the calibration factors for average-power heating and electrical heating, respectively. Based on Eq. (9), the calibration factors predicted by the three-dimensional cavity model were used to calculate the inequivalence between laser heating and electrical heating. The calculated inequivalence is 0.42% for the deposited energy of 9 J and 0.40% for the deposited energy of 5 J. Hence, the inequivalence of the 193-nm laser calorimeter is about 0.4% for the deposited energy from 9 to 5 J.

Conclusions

The equivalence between pulsed-laser heating and average-power laser heating was investigated using an axisymmetric full cavity model. The relative differences of the temperature rise and its integration at the front opening of the cavity and the edge of the cavity end are about 0.03%. The axisymmetric modeling establishes the equivalence between the pulsed-laser heating and average-power heating. Therefore, the average-power laser heating was employed to calculate the calibration factor for pulsed-laser heating conditions.

A three-dimensional full cavity model was developed to predict the calibration factors for laser heating and electrical heating. Based on the experimental data for electrical heating, a high convection coefficient for the initial heating process was predicted as a result of the transient and nonuniform temperature distributions. A low convection coefficient for the cooling process was observed because the surrounding nitrogen was heated as energy was injected into the calorimeters. The convection coefficients obtained from the experimental data were used to model the corresponding average-power laser heating, and the calibration factors for laser heating were predicted. The inequivalence of the 193-nm laser calorimeter was estimated to be 0.4% based on the results of the three-dimensional modeling. The theoretical prediction provides a quantitative estimate of the inequivalence and helps evaluate the overall uncertainty of the pulsed-laser calorimeter.

Acknowledgments

The authors thank Thomas Scott and Rodney Leonhardt for valuable contributions. Z. M. Zhang is grateful to the National Science Foundation for the support through a PECASE award.

References

[1]West, E. D., Case, W. E., Rasmussen, A. L., and Schmidt, L. B., "A Reference Calorimeter for Laser Energy Measurements," *Journal of Research of the National Bureau of Standards*, Vol. 76A, No. 1, 1972, pp. 13–25.

[2]West, E. D., and Churney, K. L., "Theory of Isoperibol Calorimetry for Laser Power and Energy Measurements," *Journal of Applied Physics*, Vol. 41, No. 6, 1970, pp. 2705–2712.

[3]Scott, T. R., "NBS Laser Power and Energy Measurements," *Proceedings of the Society of Photo-Optical Instrumentation Engineers*, Vol. 888, Society of Photo-Optical Instrumentation Engineers, Bellingham, WA, 1988, pp. 48–54.

[4]Franzen, D. L., and Schmidt, L. B., "Absolute Reference Calorimeter for Measuring High Power Laser Pulses," *Applied Optics*, Vol. 15, No. 12, 1976, pp. 3115–3122.

[5]Leonhardt, R. W., and Scott, T. R., "Deep-UV Excimer Laser Measurements at NIST," *Proceedings of the Society of Photo-Optical Instrumentation Engineers*, Vol. 2439, Society of Photo-Optical Instrumentation Engineers, Bellingham, WA, 1995, pp. 448–459.

[6]Leonhardt, R. W., "Calibration Service for Laser Power and Energy at 248 nm," National Inst. of Standards and Technology, NIST Technical Note 1394, U.S. Government Printing Office, Washington, DC, 1998.

[7]Dowell, M. L., Cromer, C. L., Leonhardt, R. W., and Scott, T. R., "Deep Ultraviolet Laser Metrology for Semiconductor Photolithography," *Characterization and Metrology for ULSI Technology*, American Inst. of Physics, CP 449, College Park, MD, 1998, pp. 539–541.

[8]Lerner, E. L., "Durable Excimer Lasers Find New Applications," *Laser Focus World*, Vol. 34, No. 7, 1998, pp. 131–135.

[9]Jain, K., *Excimer Laser Lithography*, Society of Photo-Optical Instrumentation Engineers Press, Bellingham, WA, 1990.

[10]Rhodes, Ch. K., and Hoff, P. W., "Applications of Excimer Systems," *Excimer Lasers*, Springer-Verlag, Berlin, 1979, pp. 175–188.

[11]Burns, G. W., Scroger, M. G., Strouse, G. F., Croarkin, M. C., and Guthrie, W. F., *Temperature-Electromotive Force Reference Functions and Tables for the Letter-Designated Thermocouple Types Based on the ITS-90*, U.S. Government Printing Office, Washington, DC, 1993, p. 104.

[12]Incropera, F. P., and DeWitt, D. P., *Fundamentals of Heat and Mass Transfer*, 4th ed., Wiley, New York, 1996, Chaps. 2 and 9, and Appendix A.

[13]Touloukian, Y. S., and Buyco, E. H. (eds.), *Specific Heat: Metallic Elements and Alloys, Thermophysical Properties of Matter*, Vol. 4, IFI/Plenum, New York, 1970, pp. 392–402.

[14]Touloukian, Y. S., Powell, R. W., Ho, C. Y., and Klemens, P. G. (eds.), *Thermal Conductivity: Metallic Elements and Alloys, Thermophysical Properties of Matter*, Vol. 1, IFI/Plenum, New York, 1970, pp. 561–567, 697–699.

[15]Touloukian, Y. S., and DeWitt, D. P. (eds.), *Thermal Radiative Properties: Nonmetallic Solids, Thermophysical Properties of Matter*, Vol. 8, IFI/Plenum, New York, 1972, p. 1569.

[16]McGreer, M., "Total Emittance Test Report," DSET Labs Inc., Phoenix, AZ, 1998.

[17]Chen, D. H., and Zhang, Z. M., "Thermal Analysis of the Volume Absorber in Pulsed Excimer Laser Calorimeters," *International Journal of Heat and Mass Transfer*, Vol. 43, No. 17, 2000, pp. 3061–3072.

[18]ANSYS, Inc., ANSYS Ver. 5.6, Canonsburg, PA, 1999.

[19]Chen, D. H., "Thermal Modeling and Analysis of 193 nm Pulsed Excimer Laser Calorimeters," Ph.D. Dissertation, Dept. of Mechanical Engineering, Univ. of Florida, Gainesville, May 2001.

[20]Joseph, D. D., and Preziosi, L., "Heat Waves," *Reviews of Modern Physics*, Vol. 61, No. 1, 1989, pp. 41–73.

[21]Özişik, M. N., and Tzou, D. Y., "On the Wave Theory in Heat Conduction," *Journal of Heat Transfer*, Vol. 116, No. 3, 1994, pp. 526–535.

[22]Weast, R. C., and Astle, M. J. (eds.), *CRC Handbook of Chemistry and Physics*, 60th ed., CRC Press, Boca Raton, FL, 1981, p. E-47.

[23]Touloukian, Y. S. (ed.), *Thermophysical Properties of High Temperature Solid Materials*, Vol. 4, Macmillan, New York, 1967, p. 1655.